

# Imbalance in Balance: Online Concept Balancing in Generation Models

Yukai Shi<sup>1,2</sup>Jiarong Ou<sup>2</sup>Rui Chen<sup>2</sup>Haotian Yang<sup>2</sup>Jiahao Wang<sup>2</sup>Xin Tao<sup>2†</sup>Pengfei Wan<sup>2</sup>Di Zhang<sup>2</sup>Kun Gai<sup>2</sup><sup>1</sup> Tsinghua University<sup>2</sup> Kuaishou Technology

Figure 1. **Our method achieves better concept composition ability with much smaller dataset (31M).** Existing models face missing object, attribute leakage, and concept entanglement problem. Specifically, Figure(a)(b) miss the expected concepts (twins, feather). Figure(c)(d) incorrectly match the attribute of the subjects. Figure(e)(f) exists unnecessary concepts (fork, legs).

## Abstract

In visual generation tasks, the responses and combinations of complex concepts often lack stability and are error-prone, which remains an under-explored area. In this paper, we attempt to explore the causal factors for poor concept responses through elaborately designed experiments. We also design a concept-wise equalization loss function (IMBA loss) to address this issue. Our proposed method is online, eliminating the need for offline dataset processing, and requires minimal code changes. In our newly proposed complex concept benchmark Inert-CompBench and two other public test sets, our method significantly enhances the concept response capability of baseline models and yields highly competitive results with only a few codes.

## 1. Introduction

In recent years, visual generative models have witnessed remarkable progress, attributed to the improvements of gen-

eration paradigms (e.g. diffusion models [28, 47], auto-regressive models [23, 25, 48, 49, 56]), the proposal of new network architectures (e.g. DiT [6, 12, 37], etc.), and the release of large-scale dataset (e.g. [8, 45, 51], etc.). Driven by the concerted efforts of academia, industry, and the community, these models have reached a high level of sophistication. They are now capable of generating strikingly realistic images ([2, 12, 33, 38, 43, 44]), videos ([3, 17, 22, 30, 32]), and 3D models ([26, 54, 57]), and have been extensively adopted in creative endeavors and content generation scenarios. Remarkably, the most attractive aspect of generative models is their proficiency in deciphering and recombining real-world concepts. This enables them to conjure up objects and scenes that do not even exist in the physical world. This distinctive capability significantly expands the creative boundaries for content producers, unlocking novel opportunities for innovation.

However, in real-world applications, generative models often struggle to consistently generate outputs that closely match user expectations, especially in the realm of con-

<sup>†</sup> Corresponding author.

cept composition. Consider text-to-image (T2I) generation: even the most advanced models [2, 12, 14, 33] often suffer from problems like *concept missing*, *attribute leakage* and *concept coupling* as shown in Figure 1. To address these issues, several training-free approaches [5, 7, 13, 29, 52] have been proposed. Although these methods can be effective in specific scenarios, we contend that several essential problems underlying this challenge still remain under-explored:

**Causal Factors** Visual generation models are complex systems with multiple components, and their performance is affected by many factors. Previous efforts [34, 53, 60] have yielded interesting insights, often using simple synthetic data (*e.g.* basic shapes of different sizes and colors) or focusing on class-to-image (C2I) tasks. However, these data are too simplistic to mirror the true complexity of text-to-image (T2I) tasks, where the number of concepts and their combinations far exceed those studied before. To bridge this gap, we are the first to conduct in-depth analysis on large-scale text-image pair data. We propose and verify the following hypotheses one by one: 1) When the dataset reaches a sufficient scale, concepts will naturally be covered and learned comprehensively. 2) As the model size increases, it becomes easier for the model to learn concept responses effectively. 3) The distribution of the dataset itself plays a dominant role. Through elaborately designed experiments, we have uncovered some intriguing findings. Firstly, an increase in dataset scale does not lead to improved responses for combined concepts. Secondly, once the model size reaches a certain threshold, there is no further enhancement in complex concept responses. Thirdly, a more balanced data distribution can significantly boost the model’s ability to respond to combined concepts.

**The Panacea** Based on previous analysis, our work, like prior studies [19, 24], focuses on optimizing data distribution. However, this endeavor is rife with challenges. First, the large data scale in text-to-image (T2I) tasks renders any preprocessing for dataset-level statistical analysis and equalization [21, 55] prohibitively costly. Second, since each text prompt typically contains multiple concepts, sample equalization using loss weights [9, 36] has limited effectiveness in balancing concept distributions. Third, given the diverse generation paradigms and high model training costs, an ideal solution should be plug-and-play and applicable across different models.

In this paper, we introduce a **concept-wise** equalization approach. First, we acknowledge the **imbalance** within the seemingly **balanced** dataset, where the distribution of concepts in the training data is uneven. By taking this into account, we ingeniously approximate the ideal balanced distribution using IMBA distance, which effectively captures the data distribution with unconditional generation results. Then, we develop a token-wise reweighting strategy (*a.k.a*

IMBA loss) for training. Our method is simple: it only requires a few lines of code to modify the loss function, without significant changes to the training process, and is compatible with various diffusion models.

**Evaluation** Unlike general image generation benchmarks, the ability to combine concepts can only be differentiated on more complex and targeted test sets. In addition to evaluating on existing benchmarks such as T2I-CompBench [18] and LC-Mis benchmark [60], we have carefully constructed a new benchmark called Inert-CompBench. We identify inert concepts (difficult to integrate with other concepts) from large-scale text-image datasets and combine them with head concepts to obtain caption candidates. Then we construct a concept graph and filter out the uncommon-sense compliant concept pairs based edge weight. Finally, we generate 5 captions for each pairs with LLM [1] for evaluation.

In summary, our contributions are as threefold:

- We illustrate that once the model and training data attains a substantial scale, data distribution becomes the primary determinant of the model’s concept composition ability.
- We propose the concept-wise equalization approach (IMBA loss) to address imbalanced concept distribution in training data. It is easy to implement, cost-effective, and applicable to different models. Promising results were obtained on three benchmarks.
- We introduce a novel concept composition benchmark named Inert-CompBench. This benchmark encompasses concepts that pose challenges for composition in an open-world scenario, complementing existing benchmarks.

## 2. Related Work

### 2.1. Concept Composition

Concept composition is the ability of generative models to accurately generate content with multiple concepts, reflecting their learning and understanding capabilities. It is a crucial indicator of a model’s generalization ability. In text-image generation, several benchmarks [5, 18, 60] have been proposed to comprehensively evaluate this ability. However, as shown in Figure 1, existing pre-trained models [2, 12, 33, 38] still suffer from issues like missing object, attribute leakage and concept entanglement. Some studies [4, 34, 53] based on synthetic experiments find that the concept composition ability of diffusion models is related to data completeness, balance, and disentanglement. However, these studies are often small-scale and class-conditioned, creating a gap with text-image tasks. From an application perspective, some works [5, 13, 29, 52] propose training-free methods by optimizing attention maps to enhance the model’s concept response strength, when others [11, 31] add input modalities or generating through multiple rounds of feedback. These methods are often limited

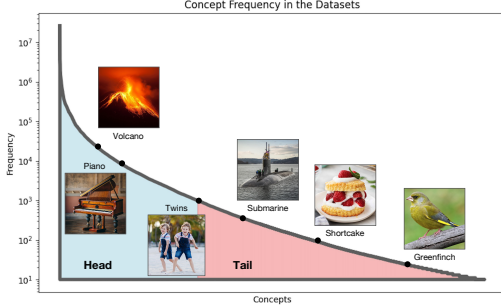


Figure 2. Concept distribution of the datasets, which follows long-tail distribution.

by the capabilities of the foundation model. And there is little work analyzing the factors determining concept composition ability from a pre-training perspective. Our work aims to address these gaps.

## 2.2. Data Balancing

Data balancing aims at learning generalized models from long-tailed data distributions. Many works [19, 24, 59] have achieved excellent results in class-specific tasks, such as resampling, re-margining, and re-weighting [9, 27, 36, 42]. Some studies [21, 39, 50, 55, 58] have extended class-based re-weighting to class-image generation tasks with inter-class distance, balanced distribution, label augmentation, or self-guided methods, showing impressive results. However, since text prompts is a joint distribution of multiple classes and each image cannot be assigned a single class, data balancing in text-image tasks still needs further exploration.

## 3. Causal Factors of Concept Composition

In this section, we bridge the gap between synthetic experiments [4, 34, 53] and text-image generation tasks to further explore the causal factors of concept composition. We conduct controlled experiments on text-image datasets and investigate the influence of crucial factors: model size, dataset scale, and data distribution.

**Experiment Setup** To ensure dataset the same and training efficiency, we re-caption open-source datasets [45] and collect a higher quality dataset, as existing open-source pre-trained models [2, 12, 33] do not provide their training data. Our dataset contains 31M text-image pairs with an average text length of 100 words and 20K noun concepts with distributions shown in Figure 2. To ensure the generality of the conclusion, we employ a DiT-based diffusion model [37] without any special design. To accurately evaluate the model’s concept composition ability rather than clarity, we introduce VQA based on VLM [35] for success rate as a quantitative metric except the CLIP-Score [40]. We detect all noun concepts in the caption and pair them, requiring the VLM to verify the existence and relationships of concepts with the following questions: “*Is concept A*

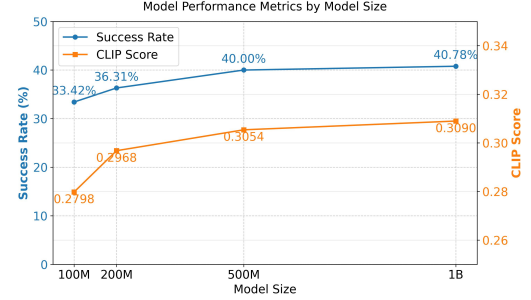


Figure 3. The performance of models with different parameter sizes under the LC-Mis benchmark [60].

*present in the image?*”, “*Is concept B present in the image?*” and “*Does the relationship between concepts A and B match the caption?*”. When all responses are “yes,” the sample is considered successful.

**Model Size** In generation tasks, model size also follows the scaling law [20], where models with more parameters have stronger generation ability. We keep the VAE from Stable Diffusion [12] the same and train diffusion models with 100M, 200M, 500M and 1B parameters on the same 31M dataset from scratch, differing only in the number of blocks and channels. We evaluate the CLIP score and success rate on the LC-Mis benchmark, as shown in Figure 3. When the model size exceeds 200M, the concept composition ability increases at a much slower rate as the model size grows. It indicates that model size is no longer the causal factor for concept composition when it reaches a certain magnitude relative to the dataset.

**Dataset Scale** It need to be clarified that the dataset scale here only refers to the number of samples for the same concept, not the co-occurrence of different concepts or data coverage, which we attribute to data distribution. To control for the same data distribution, we select two concepts from the dataset that have never co-occurred to form a pair, and extract the data containing them to create a new dataset with an imbalanced distribution. Then we maintain the sample ratio of the two concepts and sample two subsets with different scales from the new dataset, approximately following the same distribution. Finally, we resume the model which has never seen these concepts before, and conduct supervised finetuning on the two subsets for 20K steps. We generate 25 captions for each concept pair for VQA evaluation. To eliminate randomness, we select two pairs of concept composition (“piano-submarine” and “volcano-twins”), which follow imbalanced distributions of 100:1 and 10:1 respectively. As shown in Figure 4, despite the dataset being five times larger, there is no significantly improvement on the composition ability. And the number of failure cases does not decrease with the increasing dataset scale in Table 1. Therefore, simply increasing the data scale without changing the data distribution does not enhance the model’s ability for concept combination.

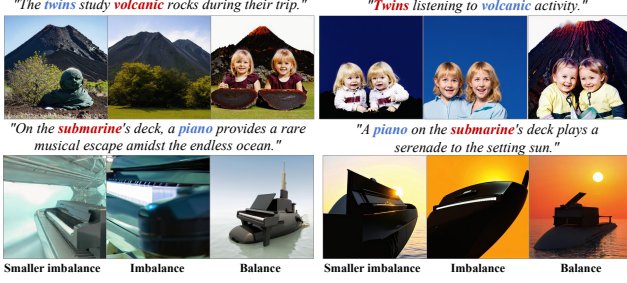


Figure 4. The performance of models with different data scales and distributions.

Pairs	piano-submarine			volcano-twins		
Head samples	3K 0.03K	15K 0.15K	0.15K 0.15K	1K 0.1K	5K 0.5K	0.5K 0.5K
Tail samples						
Success rate	16% 0.3076	20% 0.3110	56% 0.3226	28% 0.2986	20% 0.2948	64% 0.3137
CLIP Score						

Table 1. The performance of models with different data scales and distributions.

**Data Distribution** We artificially construct balanced and imbalanced datasets for the experiment. We select two concepts from the dataset that have never co-occurred to form a pair, and extract the data containing them to create a new dataset with an imbalanced distribution, serving as the imbalanced dataset. Then, we downsample the data samples of head concepts to create a balanced dataset. We also use "piano-submarine" and "twins-volcano" as concept pairs for comparison, with sample ratios of 100:1 and 10:1 in the imbalanced dataset, and 1:1 in the balanced dataset. As shown in Figure 4 and Table 1, although the imbalanced dataset contains all the data from the balanced dataset, the model trained on the balanced dataset still have stronger concept composition ability. Balanced data distribution can significantly boost the model's ability to respond to combined concepts. Additionally, when most datasets in the open-world follow a long-tail distribution, addressing the impact of data imbalance is a crucial task for improving concept composition ability.

## 4. Method

We propose an online concept-wise equalization training strategy for data balancing, ensuring both effectiveness and efficiency. We first derive the form of the loss weight from the ideal data distribution in Section 4.1. Then we propose IMBA distance as a more accurate and efficient measure of data distribution in Section 4.2. Further, we introduce the novel online token-wise IMBA loss in Section 4.3. Finally, we extract inert concepts from open-set datasets to construct the new Inert-CompBench in Section 4.4.

### 4.1. Theoretical Analysis

Without loss of generality, we derive with the  $\epsilon$ -prediction DDPM [16] framework. It is worth noting that this ap-

proach can be easily extended to various other diffusion model variants, such as flow matching [28]. In common implementations [10, 47], the training loss of diffusion models parameterized by  $\theta$  can be written as follow:

$$L = \mathbb{E}_{t, x_0, \epsilon} \|\epsilon - \epsilon_\theta(x_t, y, t)\|^2, \quad (1)$$

where  $y$  is the text prompts,  $x_t$  is the noisy image at timestep  $t$  from image  $x_0$  and random Gaussian noises  $\epsilon$ . Inspired by existing work [46] where image regions respond to prompts as concept phrases, we rewrite the loss function as follow:

$$\hat{L} = \frac{\sum_{i=1}^n \mathbb{E}_{t, \epsilon} \|\epsilon - \epsilon_\theta(a_t^i, c_i, t)\|^2 \varphi(c_i)}{\sum_{i=1}^n \varphi(c_i)}, \quad (2)$$

where  $c_i$  is a concept within the dataset containing  $n$  concepts,  $a_t^i$  is all image regions belonging to concept  $c_i$ , and  $\varphi(c_i)$  is the frequency proportion of concept  $c_i$  among all concepts. Naturally, we have  $\sum_{i=1}^n \varphi(c_i) = 1$ , and assume that the set of image regions  $A$  and the set of images  $X$  have a one-to-one and onto mapping.

We assume that the optimal balance distribution of concepts is  $\varphi^*(c_i) \sim U(1, n)$ , which follows a discrete uniform distribution. Then we are able to write the optimal loss function based on Equation 2 as follow:

$$\begin{aligned} \hat{L}^* &= \sum_{i=1}^n \mathbb{E}_{t, \epsilon} \|\epsilon - \epsilon_\theta(a_t, c_i, t)\|^2 \varphi^*(c_i) \\ &= \sum_{i=1}^n \mathbb{E}_{t, \epsilon} \|\epsilon - \epsilon_\theta(a_t, c_i, t)\|^2 \varphi(c_i) \cdot \frac{\varphi^*(c_i)}{\varphi(c_i)}, \end{aligned} \quad (3)$$

where  $\frac{\varphi^*(c_i)}{\varphi(c_i)}$  is the loss weight we wish to obtain. Since  $\varphi^*(c_i)$  is a constant when it follows a discrete uniform distribution, we only need to estimate  $\frac{1}{\varphi(c_i)}$ .

On the other hand, we wish that the model responds with similar intensity to different concepts [5]. Thus, we have the response intensity represented by the difference between the conditional and unconditional distribution as follow:

$$\|\epsilon_\theta(a_t, c_i, t) - \epsilon_\theta(a_t, \phi, t)\| = f(a_t), \quad (4)$$

where the intensity depends only on  $a_t$ . Meanwhile, we have the formulation of conditional and unconditional distribution in classifier-free guidance [15] as follows:

$$\epsilon_\theta(a_t, c_i, t) = \nabla_{a_t} \log p(a_t) + \sigma_t \nabla_{a_t} \log p(c_i | a_t), \quad (5)$$

$$\epsilon_\theta(a_t, \phi, t) = \nabla_{a_t} \log p(a_t) + \sigma_t \nabla_{a_t} \log p(\phi | a_t). \quad (6)$$

During training, the unconditional distribution is trained on the weighted expectation of multiple concepts:

$$\begin{aligned} \epsilon_\theta(a_t, \phi, t) &= \frac{\sum_{i=1}^n \varphi(c_i) [\nabla_{a_t} \log p(a_t) + \sigma_t \nabla_{a_t} \log p(c_i | a_t)]}{\sum_{i=1}^n \varphi(c_i)} \\ &= \nabla_{a_t} \log p(a_t) + \frac{\sigma_t \sum_{i=1}^n \varphi(c_i) \nabla_{a_t} \log p(c_i | a_t)}{\sum_{i=1}^n \varphi(c_i)}. \end{aligned} \quad (7)$$

Then we apply Equation 5, 6 and 7 into Equation 4:

$$\begin{aligned}
D_j &= \|\epsilon_\theta(a_t, c_i, t) - \epsilon_\theta(a_t, \phi, t)\| \\
&= \|\sigma_t \nabla_{a_t} \log p(c_j | a_t) - \sigma_t \nabla_{a_t} \log p(\phi | a_t)\| \\
&= \left\| \sigma_t \nabla_{a_t} \log p(c_j | a_t) - \frac{\sigma_t \sum_{i=1}^n \varphi(c_i) \nabla_{a_t} \log p(c_i | a_t)}{\sum_{i=1}^n \varphi(c_i)} \right\| \\
&= \left\| \frac{\sigma_t}{\sum_{i=1}^n \varphi(c_i)} \left[ \nabla_{a_t} \log p(c_j | a_t) - \sum_{i=1, i \neq j}^n \varphi(c_i) \right. \right. \\
&\quad \left. \left. - \sum_{i=1, i \neq j}^n \varphi(c_i) \nabla_{a_t} \log p(c_i | a_t) \right] \right\| \propto \frac{1}{\varphi(c_j)},
\end{aligned} \tag{8}$$

where  $D_j$  is the difference between the conditional and unconditional distributions of concept  $c_j$ , and we refer it as **IMBA distance**. Since it is positively correlated with  $\frac{1}{\varphi(c_i)}$ , we use it to represent the frequency proportion of the concept in the dataset. Then we apply Equation 8 into Equation 3 to obtain optimal loss:

$$\begin{aligned}
\hat{L}^* &= \sum_{i=1}^n \mathbb{E}_{t,\epsilon} \|\epsilon - \epsilon_\theta(a_t, c_i, t)\|^2 \varphi(c_i) \cdot \frac{\varphi^*(c_i)}{\varphi(c_i)} \\
&= \sum_{i=1}^n \mathbb{E}_{t,\epsilon} \|\epsilon - \epsilon_\theta(a_t, c_i, t)\|^2 \\
&\quad \|\epsilon_\theta(a_t, c_i, t) - \epsilon_\theta(a_t, \phi, t)\|_{sg}^\gamma \varphi(c_i) \\
&\doteq \sum_{i=1}^n \mathbb{E}_{t,\epsilon} \|\epsilon - \epsilon_\theta(a_t, c_i, t)\|^2 \|\epsilon - \epsilon_\theta(a_t, \phi, t)\|_{sg}^\gamma \varphi(c_i),
\end{aligned} \tag{9}$$

where we replace conditional distribution  $\epsilon_\theta$  with ground truth  $\epsilon$  for training stability. Finally, we rewrite loss function back to image  $x$  and text prompts  $y$ :

$$D = \|\epsilon - \epsilon_\theta(x_t, \phi, t)\|_{sg}^\gamma, \tag{10}$$

$$L^* = \mathbb{E}_{t,x_0,\epsilon} D \|\epsilon - \epsilon_\theta(x_t, y, t)\|^2, \tag{11}$$

where we implement the distance with  $L - \gamma$  norm, and stopping gradient during training. We refer the novel loss function as **IMBA loss**. IMBA loss adapts dynamically during the training process without additional off-line modeling, ensuring both effectiveness and efficiency.

## 4.2. IMBA Distance

Measuring data balance is particularly challenging due to the complexity of text prompts compared to classes [27, 39]. Additionally, with the exponential growth of datasets, offline data pruning will lead to data waste and significant computational and time costs. In this section, we demonstrate that the IMBA distance is able to represent the frequency proportion of concepts with both synthetic experiments and text-image generation experiments. We further give out the formulation of IMBA distance in Appendix A.

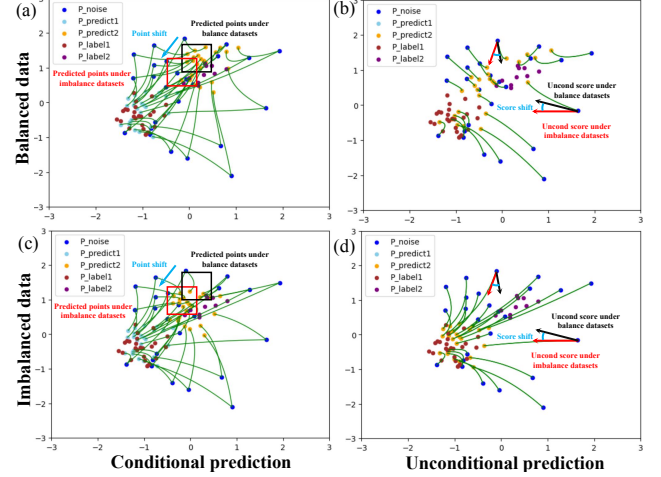


**Figure 5. Comparison between results from balance and imbalance datasets.** We simulate the training and inference results of diffusion models in a 2-dimensional space. With the dataset consisted by two classes (brown and purple points), diffusion models map random noise(blue points) to the prediction(yellow points) with flow matching(green curve). Comparing Figure (a) and (c), imbalanced data leads to a **shift** from **black box** to **red box** on the prediction of tail concepts, harming the generalization of the tail concept(purple points). Comparing Figure (b) and (d), imbalanced data makes unconditional score distribution tilt towards the head concept(brown points) from **black arrow** to **red arrow**, proving that the difference between unconditional and conditional score distributions can serve as a metric for dataset distribution.

### 4.2.1. Synthetic Experiments

As shown in Figure 5, we simulate the training and inference results of diffusion models in a 2-dimensional space. All data samples are represented by 2-dimensional coordinates and initialized into two classes, following normal distributions  $P_1 \sim U(-1, -0.3, 0.1, 0.1, 0)$  (**brown points**) and  $P_2 \sim U(0.3, 1, 0.1, 0.1, 0)$  (**purple points**), respectively. We construct balanced and imbalanced training sets, both with 10K sample points in total, but with Class 1 (**brown points**): Class 2 (**purple points**) ratios of 1:1 and 99:1 respectively. Then we train a diffusion model with a 2-layer MLP on both datasets. During inference, random noise points (**blue points**) following a standard normal distribution are mapped to the two target distributions through flow (**green curve**) matching conditioned on the class, resulting in predicted points (**sky blue** and **yellow**). In Figure 5, figure (a,b) / (c,d) show the results of (conditional, unconditional) inference under balanced / imbalanced data respectively.

Comparing figures (a) and (c), we find that despite conditioning on the class during inference, the imbalanced data still pulls the prediction results (**yellow points**) of the tail concept (**purple points**) towards the head concept (**brown points**). This is specifically shown by the predicted points

Head concepts	man	girl	cat	koala
Frequency	1.8M	365K	180K	2.7K
Tail concepts	gramophone	jeep	submarine	greenfinch
Frequency	756	420	332	24

Table 2. The frequency of concepts in the training set.

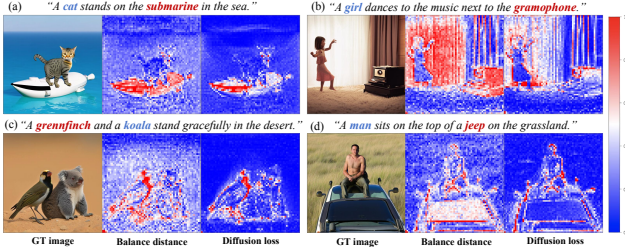


Figure 6. **IMBA distance and diffusion loss of different concepts.** Tail concepts (**red words**) tend to have larger IMBA distance and diffusion loss than head concepts (**blue words**).

in the **black box** in Fig.(a) drifting into the **red box** in Fig.(c) under the imbalanced data. This indicates that an imbalanced dataset harms the generalization of the tail concept. Meanwhile, comparing Fig.(b) and (d), we observe that under the balanced dataset, the unconditional score distribution points to the middle of the two classes (**black arrow** in Fig.(b)). But under the imbalanced dataset, it directly points to the head concept (**red arrow** in Fig.(d)), showing a very obvious score shift (**blue curve**). This demonstrates that the unconditional score distribution tends to favor the head concept under an imbalanced dataset, reducing the difference between the head concept’s conditional distribution and unconditional distribution, consistent with the analysis in Equation 10. Therefore, the IMBA distance can serve as a self-equilibrated, effective and efficient metric for data distribution during the training process.

#### 4.2.2. Text-image Generation Experiments

In this section, we further demonstrate that IMBA loss can serve as the measure of data distribution on text-image experiments. We first collect a list of concepts from the training set with head and tail concepts each accounting for half in Table 2. Then, we pair head and tail concepts to create new captions to generate composition images. We select plausible samples to calculate IMBA distance and diffusion loss. In Equation 10, since IMBA distance is related to  $a_t$ , it is not comparable under different content and timesteps. Therefore, we chose  $t = 1000$ , when the entire image is random noise, to compare the IMBA distance of different concepts. We normalize both IMBA distance and diffusion loss to  $[0, 1]$ , with the red area indicating larger values compared to the blue area. As shown in Figure 6, we find that tail concepts generally exhibit a larger IMBA distance compared to head concepts, which demonstrate that IMBA distance can measure the data distribution. Additionally, the

---

#### Algorithm 1 Training with IMBA loss

---

**Require:** Dataset  $\{\mathbf{X}, \mathbf{Y}\}$ , noise scheduler  $\bar{\alpha}$ , model  $\epsilon_\theta$

- 1: **repeat**
  - 2:     Sample data  $(x_0, y) \sim \{\mathbf{X}, \mathbf{Y}\}$
  - 3:     Sample noise  $\epsilon \sim \mathcal{N}(0, 1)$  and time  $t \sim \mathbf{U}(0, 1)$
  - 4:     Add noise with  $x_t = \sqrt{\bar{\alpha}_t}x_0 + \sqrt{1 - \bar{\alpha}_t}\epsilon$
  - 5:     **Calculate weight**  $D = \|\epsilon - \epsilon_\theta(x_t, \phi, t)\|_{sg}^\gamma$
  - 6:     Conditional loss  $L^* = D \|\epsilon - \epsilon_\theta(x_t, y, t)\|^2$
  - 7:     Unconditional loss  $L_u = \|\epsilon - \epsilon_\theta(x_t, \phi, t)\|^2$
  - 8:     Compute loss  $L = \lambda L^* + (1 - \lambda)L_u$
  - 9:     Back propagation  $\theta = \theta - \eta \nabla_\theta L$
  - 10: **until** converged
- 

diffusion loss is larger for tail concepts, indicating that they are under-fitting than head concepts. We further give out the formulation of IMBA distance in Appendix A.

#### 4.3. IMBA Loss

Here we present the process of our IMBA loss in Algorithm 1. During training, after adding noise  $\epsilon$  to the image  $x_0$  to obtain  $x_t$ , we use the diffusion model  $\theta$  to predict the conditional score  $\epsilon_\theta(x_t, y, t)$  and the unconditional score  $\epsilon_\theta(x_t, \phi, t)$ . The unconditional score and ground truth noise are used to calculate the IMBA distance  $D$  based on the Equation 10 with stopping gradient. Then the IMBA distance weights the conditional loss from the conditional score and ground truth, resulting in the final IMBA loss  $L^*$ . Since the model also needs to train the unconditional distribution, we use the previously obtained unconditional score to calculate the loss, applying a weighting coefficient  $\lambda$  to replace the original random drop condition. In the specific implementation, we set  $\gamma = 0.8$  to avoid color shifts and  $\lambda = 0.9$  which is the same as the mask ratio of the condition in the original diffusion training. The IMBA distance typically has a shape of  $(B, N, C)$ , and we find that averaging over the channel dimension benefits training stability.

Compared to offline concept frequency-based loss weights [9, 36, 59], IMBA loss is more accurate and efficient. Firstly, since text prompts are the joint distribution of multiple concepts, and each concept has a different frequency, it is challenging to intuitively and quickly set loss weights for samples as in class-related tasks. Secondly, while it is feasible to construct a concept graph where concepts are represented as nodes and the co-occurrence frequency of concept pairs as edge values to derive loss weights, the data distribution that the model learns evolves throughout the training process. This evolution creates a misalignment between the offline loss weights and the model’s understanding. In contrast, IMBA distance is naturally coupled with the training process, providing a more consistent representation of data distribution. Thirdly, since different regions of an image may contain different con-

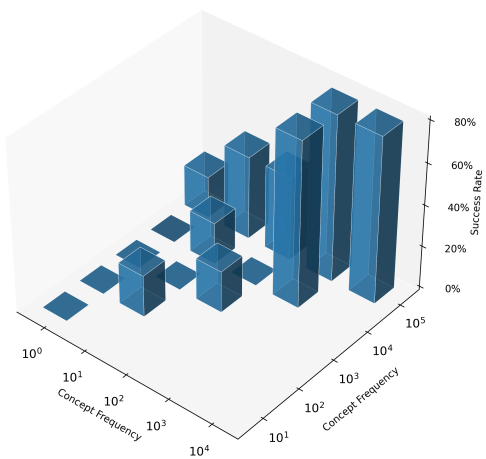


Figure 7. Success rate of concepts with different frequency. Tail concepts have lower success rate than head concepts.

cepts, data balancing should be performed at the concept region level. IMBA loss supports different loss weights for different regions, making it more accurate compared to a single weight for all regions. Additionally, with the exponential growth of data, constructing an offline concept graph becomes increasingly time-consuming and computationally intensive, making it challenging to reuse across different datasets. IMBA loss, on the other hand, only requires the calculation of IMBA distance with only a few lines of code during training, making it highly efficient and easily reusable. It is worth noting that our method is orthogonal to training-free methods and can be combined to further enhance the concept composition ability.

#### 4.4. Inert-CompBench

Based on the analysis in Section 3, we further discover that some low-frequency concepts in datasets are difficult to successfully composite with other concepts, which we refer to as inert concepts. We first calculate the frequency of all noun concepts in the dataset, and sample 6 concepts uniformly from each frequency interval after taking the logarithm. Then we combine them in pairs to obtain 15 pairs and generate 5 captions for each pair with 75 captions in total. We evaluate the failure rate on the baseline models in Figure 7. We find that the success rate of concept composition increases as the concept frequency increases, indicating that tail concepts are more prone to failure cases compared to head concepts. Therefore, we should place more emphasis on tail concepts when constructing benchmarks.

Due to the lack of attention to these concepts in existing benchmarks [18, 60], we extract inert concepts from open-world datasets to construct a new benchmark called Inert-CompBench as a supplement. As shown in Algorithm 2, our framework comprises five phases: (1) Extract candidate sets where head concepts exhibit occurrence frequen-

---

#### Algorithm 2 Inert-CompBench Construction

---

**Require:** Dataset  $\mathcal{D}$ , concept count  $n$ , combination size  $k$

- 1: Extract head concepts  $\mathcal{H}$  and tail concepts  $\mathcal{T}$  from  $\mathcal{D}$  where  $\text{freq}(\mathcal{H})/\text{freq}(\mathcal{T}) > 100$  *(Phase 1)*
- 2: Select  $n$  representative entities:  $\hat{\mathcal{H}} \subset \mathcal{H}, \hat{\mathcal{T}} \subset \mathcal{T}$  via semantic typicality analysis *(Phase 2)*
- 3: Generate Cartesian product space  $\mathcal{C} = \hat{\mathcal{H}} \times \hat{\mathcal{T}}$  with  $|\mathcal{C}| = n^2$  *(Phase 3)*
- 4: Build co-occurrence graph  $G$  from  $\mathcal{D}$ , select  $\mathcal{C}^* = \text{Top-}k$  pairs with minimal edge weights in  $G$  *(Phase 4)*
- 5: Generate prompts  $\mathcal{P} = \bigcup_{c \in \mathcal{C}^*} \text{GPT-4}(c, 5)$ , yielding  $|\mathcal{P}| = 1k$  *(Phase 5)*

**Ensure:** Benchmark set  $\mathcal{B} = \{\mathcal{P}, \mathcal{C}^*\}$

---

cies exceeding tail concepts by 100:1 ratio based on large-scale dataset statistics. (2) Select  $n$  domain-representative entity concepts from each pool through semantic typicality analysis. (3) Construct  $n \times n$  Cartesian product combination space. (4) Build concept co-occurrence graphs to filter Top-K pairs with minimal structural associations, ensuring test cases reflect non-trivial compositional relationships. (5) Generate 5 linguistically diverse prompts per selected pair using GPT-4, ultimately forming a benchmark with 1K fine-grained test instances. This design forces models to handle statistically weak concept combinations, effectively revealing their compositional reasoning limitations.

## 5. Experiments

**Setup.** To keep the dataset the same and improve training efficiency, we re-capture and filter open-source data [45], resulting in a higher quality dataset of 31M samples for training. We employ a 1B parameter DiT-based diffusion model [37] without any special design as the pipeline. Text prompts are injected into the diffusion model using T5 model [41], and  $512 \times 512$  images are encoded into the latent space using the VAE from Stable Diffusion [12].

**Baseline.** We train the diffusion model from scratch for 4 epochs on the new dataset using the original diffusion loss to establish a baseline. To demonstrate the effectiveness of our method, we train the same model for the same epochs on the same dataset with the proposed IMBA loss. Additionally, we implement the training-free method [5] on the baseline for comparison. Furthermore, we finetune the baseline model from 3 epochs for 1 additional epochs with the IMBA loss, demonstrating that our method also provides significant benefits during fine-tuning.

**Benchmark.** We evaluate the concept composition ability of models on T2I-CompBench [18], LC-Mis [60] and Inert-CompBench. We employ VQA based on VLM [35] for evaluation in LC-Mis and Inert-CompBench as described in experiments setup of Section 3.

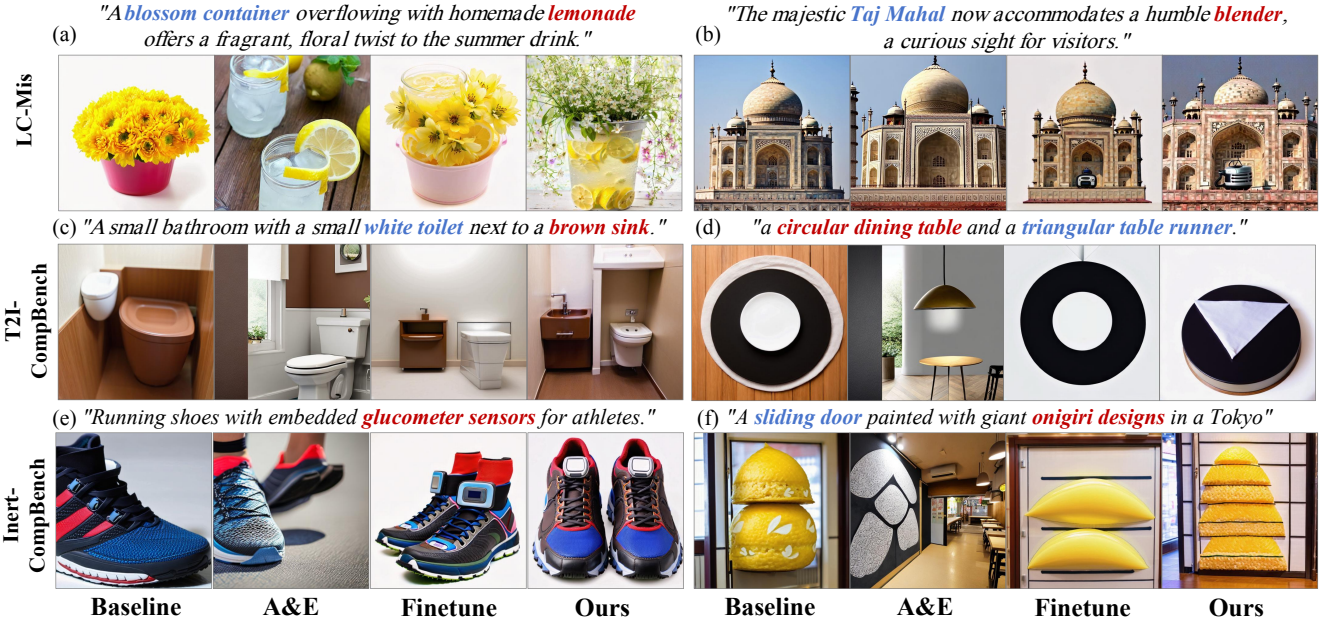


Figure 8. Qualitative comparison with baseline.

Model	LC-Mis [60]		T2I-CompBench [18]					Inert-CompBench	
	CLIP Score ↑	VQA ↑	Color ↑	Shape ↑	Texture ↑	Non-spatial ↑	Spatial ↑	CLIP Score ↑	VQA ↑
Baseline	0.3045	46.21%	0.5812	0.4307	0.6188	0.3041	0.1966	0.3194	44%
A&E [5]	<b>0.3198</b>	48.42%	0.6141	0.4378	0.6329	<b>0.3078</b>	0.1998	<b>0.3303</b>	44.5%
Finetune	0.3073	<u>51.82%</u>	<u>0.6668</u>	<u>0.4919</u>	<u>0.6575</u>	<u>0.3075</u>	<u>0.2218</u>	0.3172	<u>46%</u>
Ours	0.3121	<b>62.89%</b>	<b>0.7067</b>	<b>0.5151</b>	<b>0.6861</b>	0.3071	<b>0.2518</b>	0.3229	<b>57%</b>

Table 3. Quantitative comparison with baseline. **Bold** font indicates the optimal value, and underlining indicates the second-best value.

## 5.1. Quantitative Comparison

As shown in Table 3, we compare baseline, A&E [5], finetuning, and from-scratch training of our IMBA loss on LC-Mis [60], T2i-CompBench [18] and ours Inert-CompBench. Compared with the diffusion loss in the baseline, our IMBA loss can significantly improve the concept composition ability, whether training from scratch or finetuning from a pre-trained model. In addition, training from scratch yields better results compared to fine-tuning. Besides, when our approach achieves similar improvements in object missing, A&E [5] performs slightly better on CLIP score, but far worse on attribute leakage (shape,color,texture,VQA). This is because A&E is limited by the foundational generation model and cannot generate concepts that the generation model does not understand. Meanwhile, since the improvement of fine-tuning on Inert-CompBench is limited, it indicates that inert concepts require a longer training process to enhance concept composition ability.

## 5.2. Qualitative Comparison

In Figure 8, we visualize the comparison results on three benchmarks separately, demonstrating the superiority of our method. We not only address object missing and attribute leakage effectively on existing benchmarks,

but also demonstrate significant advantages under Inert-CompBench, greatly improving the success rate of inert concepts.

**Ablation.** We further conduct comprehensive experiments on sample-wise loss weight, hyper-parameters and IMBA distance. Please refer to Appendix B.

## 6. Conclusion

In this work, we propose a concept-wise equalization approach called IMBA loss for concept balancing to improve the concept composition ability of generation models. We first analyze the casual factor with elaborately designed experiments, bridging the gap between synthetic experiments and large-scale text-image generation. We demonstrate that data distribution has become the key factor when the model reaches a considerable size. Then, we propose the IMBA distance to estimate data distribution and demonstrate its effectiveness through both synthetic and text-image experiments. Subsequently, we introduce an online concept-wise equalization approach IMBA loss to balance concepts. Further, we identify inert concepts (difficult to integrate with other concepts) from large-scale text-image datasets and introduce the Inert-CompBench, complementing existing benchmarks. Finally, we conduct comprehensive experiments to demonstrate the priority of our methods.

## References

- [1] Josh Achiam, Steven Adler, Sandhini Agarwal, Lama Ahmad, Ilge Akkaya, Florencia Leoni Aleman, Diogo Almeida, Janko Altenschmidt, Sam Altman, Shyamal Anadkat, et al. Gpt-4 technical report. *arXiv preprint arXiv:2303.08774*, 2023. 2
- [2] James Betker, Gabriel Goh, Li Jing, Tim Brooks, Jianfeng Wang, Linjie Li, Long Ouyang, Juntang Zhuang, Joyce Lee, Yufei Guo, et al. Improving image generation with better captions. *Computer Science*. <https://cdn.openai.com/papers/dall-e-3.pdf>, 2(3):8, 2023. 1, 2, 3
- [3] Tim Brooks, Bill Peebles, Connor Holmes, Will DePue, Yufei Guo, Li Jing, David Schnurr, Joe Taylor, Troy Luhman, Eric Luhman, Clarence Ng, Ricky Wang, and Aditya Ramesh. Video generation models as world simulators, 2024. 1
- [4] Yingshan Chang, Yasi Zhang, Zhiyuan Fang, Ying Nian Wu, Yonatan Bisk, and Feng Gao. Skews in the phenomenon space hinder generalization in text-to-image generation. In *European Conference on Computer Vision*, pages 422–439. Springer, 2024. 2, 3
- [5] Hila Chefer, Yuval Alaluf, Yael Vinker, Lior Wolf, and Daniel Cohen-Or. Attend-and-excite: Attention-based semantic guidance for text-to-image diffusion models. *ACM Transactions on Graphics (TOG)*, 42(4):1–10, 2023. 2, 4, 7, 8
- [6] Junsong Chen, Jincheng Yu, Chongjian Ge, Lewei Yao, Enze Xie, Yue Wu, Zhongdao Wang, James Kwok, Ping Luo, Huchuan Lu, et al. Pixart- $\alpha$ : Fast training of diffusion transformer for photorealistic text-to-image synthesis. *arXiv preprint arXiv:2310.00426*, 2023. 1
- [7] Minghao Chen, Iro Laina, and Andrea Vedaldi. Training-free layout control with cross-attention guidance. In *Proceedings of the IEEE/CVF winter conference on applications of computer vision*, pages 5343–5353, 2024. 2
- [8] Tsai-Shien Chen, Aliaksandr Siarohin, Willi Menapace, Ekaterina Deyneka, Hsiang-wei Chao, Byung Eun Jeon, Yuwei Fang, Hsin-Ying Lee, Jian Ren, Ming-Hsuan Yang, et al. Panda-70m: Captioning 70m videos with multiple cross-modality teachers. In *Proceedings of the IEEE/CVF Conference on Computer Vision and Pattern Recognition*, pages 13320–13331, 2024. 1
- [9] Yin Cui, Menglin Jia, Tsung-Yi Lin, Yang Song, and Serge Belongie. Class-balanced loss based on effective number of samples. In *Proceedings of the IEEE/CVF conference on computer vision and pattern recognition*, pages 9268–9277, 2019. 2, 3, 6, 12
- [10] Prafulla Dhariwal and Alexander Nichol. Diffusion models beat gans on image synthesis. In *NeurIPS*, 2021. 4
- [11] Ganggui Ding, Canyu Zhao, Wen Wang, Zhen Yang, Zide Liu, Hao Chen, and Chunhua Shen. Freecustom: Tuning-free customized image generation for multi-concept composition. In *Proceedings of the IEEE/CVF Conference on Computer Vision and Pattern Recognition*, pages 9089–9098, 2024. 2
- [12] Patrick Esser, Sumith Kulal, Andreas Blattmann, Rahim Entezari, Jonas Müller, Harry Saini, Yam Levi, Dominik Lorenz, Axel Sauer, Frederic Boesel, et al. Scaling rectified flow transformers for high-resolution image synthesis. *arXiv preprint arXiv:2403.03206*, 2024. 1, 2, 3, 7
- [13] Weixi Feng, Xuehai He, Tsu-Jui Fu, Varun Jampani, Arjun Akula, Pradyumna Narayana, Sugato Basu, Xin Eric Wang, and William Yang Wang. Training-free structured diffusion guidance for compositional text-to-image synthesis. *arXiv preprint arXiv:2212.05032*, 2022. 2
- [14] Flux. Flux [Text-to-Image Model]. <https://blackforestlabs.ai/announcing-black-forest-labs/>, 2024. 2
- [15] Jonathan Ho and Tim Salimans. Classifier-free diffusion guidance. *arXiv preprint arXiv:2207.12598*, 2022. 4
- [16] Jonathan Ho, Ajay Jain, and Pieter Abbeel. Denoising diffusion probabilistic models. *Advances in neural information processing systems*, 33:6840–6851, 2020. 4
- [17] Jonathan Ho, William Chan, Chitwan Saharia, Jay Whang, Ruiqi Gao, Alexey Gritsenko, Diederik P Kingma, Ben Poole, Mohammad Norouzi, David J Fleet, et al. Imagen video: High definition video generation with diffusion models. *arXiv preprint arXiv:2210.02303*, 2022. 1
- [18] Kaiyi Huang, Kaiyue Sun, Enze Xie, Zhenguo Li, and Xihui Liu. T2i-compbench: A comprehensive benchmark for open-world compositional text-to-image generation. *Advances in Neural Information Processing Systems*, 36:78723–78747, 2023. 2, 7, 8
- [19] Justin M Johnson and Taghi M Khoshgoftaar. Survey on deep learning with class imbalance. *Journal of big data*, 6(1):1–54, 2019. 2, 3
- [20] Jared Kaplan, Sam McCandlish, Tom Henighan, Tom B Brown, Benjamin Chess, Rewon Child, Scott Gray, Alec Radford, Jeffrey Wu, and Dario Amodei. Scaling laws for neural language models. *arXiv preprint arXiv:2001.08361*, 2020. 3
- [21] Kai Katsumata, Duc Minh Vo, and Hideki Nakayama. Label augmentation as inter-class data augmentation for conditional image synthesis with imbalanced data. In *Proceedings of the IEEE/CVF Winter Conference on Applications of Computer Vision*, pages 4944–4953, 2024. 2, 3
- [22] Kuaishou. Kling. <https://klingai.kuaishou.com>, 2024. 1
- [23] Doyup Lee, Chiheon Kim, Saehoon Kim, Minsu Cho, and Wook-Shin Han. Autoregressive image generation using residual quantization. In *Proceedings of the IEEE/CVF Conference on Computer Vision and Pattern Recognition*, pages 11523–11532, 2022. 1
- [24] Joffrey L Leevy, Taghi M Khoshgoftaar, Richard A Bauder, and Naeem Seliya. A survey on addressing high-class imbalance in big data. *Journal of Big Data*, 5(1):1–30, 2018. 2, 3
- [25] Tianhong Li, Yonglong Tian, He Li, Mingyang Deng, and Kaiming He. Autoregressive image generation without vector quantization. *Advances in Neural Information Processing Systems*, 37:56424–56445, 2024. 1
- [26] Weiyu Li, Jiarui Liu, Rui Chen, Yixun Liang, Xuelin Chen, Ping Tan, and Xiaoxiao Long. Craftsman: High-fidelity mesh generation with 3d native generation and interactive geometry refiner. *arXiv preprint arXiv:2405.14979*, 2024. 1

- [27] Tsung-Yi Lin, Priya Goyal, Ross Girshick, Kaiming He, and Piotr Dollár. Focal loss for dense object detection. In *Proceedings of the IEEE international conference on computer vision*, pages 2980–2988, 2017. 3, 5
- [28] Yaron Lipman, Ricky TQ Chen, Heli Ben-Hamu, Maximilian Nickel, and Matt Le. Flow matching for generative modeling. *arXiv preprint arXiv:2210.02747*, 2022. 1, 4
- [29] Nan Liu, Shuang Li, Yilun Du, Antonio Torralba, and Joshua B Tenenbaum. Compositional visual generation with composable diffusion models. In *ECCV*, 2022. 2
- [30] Xin Ma, Yaohui Wang, Gengyun Jia, Xinyuan Chen, Ziwei Liu, Yuan-Fang Li, Cunjian Chen, and Yu Qiao. Latte: Latent diffusion transformer for video generation. *arXiv preprint arXiv:2401.03048*, 2024. 1
- [31] Oscar Mañas, Pietro Astolfi, Melissa Hall, Candace Ross, Jack Urbanek, Adina Williams, Aishwarya Agrawal, Adriana Romero-Soriano, and Michal Drozdzał. Improving text-to-image consistency via automatic prompt optimization. *arXiv preprint arXiv:2403.17804*, 2024. 2
- [32] Willi Menapace, Aliaksandr Siarohin, Ivan Skorokhodov, Ekaterina Deyneka, Tsai-Shien Chen, Anil Kag, Yuwei Fang, Aleksei Stoliar, Elisa Ricci, Jian Ren, et al. Snap video: Scaled spatiotemporal transformers for text-to-video synthesis. *arXiv preprint arXiv:2402.14797*, 2024. 1
- [33] Midjourney. Midjourney (V5.2) [Text-to-Image Model]. <https://www.midjourney.com>, 2023. 1, 2, 3
- [34] Maya Okawa, Ekdeep S Lubana, Robert Dick, and Hidenori Tanaka. Compositional abilities emerge multiplicatively: Exploring diffusion models on a synthetic task. *Advances in Neural Information Processing Systems*, 36:50173–50195, 2023. 2, 3
- [35] OpenAI. Gpt-4v(ision) system card, 2023. 3, 7
- [36] Seulki Park, Jongin Lim, Younghan Jeon, and Jin Young Choi. Influence-balanced loss for imbalanced visual classification. In *Proceedings of the IEEE/CVF international conference on computer vision*, pages 735–744, 2021. 2, 3, 6
- [37] William Peebles and Saining Xie. Scalable diffusion models with transformers. In *Proceedings of the IEEE/CVF International Conference on Computer Vision*, pages 4195–4205, 2023. 1, 3, 7
- [38] Dustin Podell, Zion English, Kyle Lacey, Andreas Blattmann, Tim Dockhorn, Jonas Müller, Joe Penna, and Robin Rombach. Sdxl: Improving latent diffusion models for high-resolution image synthesis. *arXiv preprint arXiv:2307.01952*, 2023. 1, 2
- [39] Yiming Qin, Huangjie Zheng, Jiangchao Yao, Mingyuan Zhou, and Ya Zhang. Class-balancing diffusion models. In *Proceedings of the IEEE/CVF Conference on Computer Vision and Pattern Recognition*, pages 18434–18443, 2023. 3, 5
- [40] Alec Radford, Jong Wook Kim, Chris Hallacy, Aditya Ramesh, Gabriel Goh, Sandhini Agarwal, Girish Sastry, Amanda Askell, Pamela Mishkin, Jack Clark, et al. Learning transferable visual models from natural language supervision. In *International conference on machine learning*, pages 8748–8763. PMLR, 2021. 3
- [41] Colin Raffel, Noam Shazeer, Adam Roberts, Katherine Lee, Sharan Narang, Michael Matena, Yanqi Zhou, Wei Li, and Peter J Liu. Exploring the limits of transfer learning with a unified text-to-text transformer. *Journal of machine learning research*, 21(140):1–67, 2020. 7
- [42] Jiawei Ren, Cunjun Yu, Xiao Ma, Haiyu Zhao, Shuai Yi, et al. Balanced meta-softmax for long-tailed visual recognition. *Advances in neural information processing systems*, 33:4175–4186, 2020. 3
- [43] Robin Rombach, Andreas Blattmann, Dominik Lorenz, Patrick Esser, and Björn Ommer. High-resolution image synthesis with latent diffusion models. In *Proceedings of the IEEE/CVF Conference on Computer Vision and Pattern Recognition (CVPR)*, pages 10684–10695, 2022. 1
- [44] Chitwan Saharia, William Chan, Saurabh Saxena, Lala Li, Jay Whang, Emily L Denton, Kamayr Ghasemipour, Raphael Gontijo Lopes, Burcu Karagol Ayan, Tim Salimans, et al. Photorealistic text-to-image diffusion models with deep language understanding. *Advances in neural information processing systems*, 35:36479–36494, 2022. 1
- [45] Christoph Schuhmann, Romain Beaumont, Richard Vencu, Cade Gordon, Ross Wightman, Mehdi Cherti, Theo Coombes, Aarush Katta, Clayton Mullis, Mitchell Wortsman, et al. Laion-5b: An open large-scale dataset for training next generation image-text models. *NeurIPS*, 2022. 1, 3, 7
- [46] Gowthami Somepalli, Vasu Singla, Micah Goldblum, Jonas Geiping, and Tom Goldstein. Diffusion art or digital forgery? investigating data replication in diffusion models. In *Proceedings of the IEEE/CVF conference on computer vision and pattern recognition*, pages 6048–6058, 2023. 4
- [47] Yang Song, Jascha Sohl-Dickstein, Diederik P Kingma, Abhishek Kumar, Stefano Ermon, and Ben Poole. Score-based generative modeling through stochastic differential equations. *arXiv preprint arXiv:2011.13456*, 2020. 1, 4
- [48] Peize Sun, Yi Jiang, Shoufa Chen, Shilong Zhang, Bingyue Peng, Ping Luo, and Zehuan Yuan. Autoregressive model beats diffusion: Llama for scalable image generation. *arXiv preprint arXiv:2406.06525*, 2024. 1
- [49] Keyu Tian, Yi Jiang, Zehuan Yuan, Bingyue Peng, and Liwei Wang. Visual autoregressive modeling: Scalable image generation via next-scale prediction. *Advances in neural information processing systems*, 37:84839–84865, 2024. 1
- [50] Soobin Um and Jong Chul Ye. Self-guided generation of minority samples using diffusion models. In *European Conference on Computer Vision*, pages 414–430. Springer, 2024. 3
- [51] Qiuhe Wang, Yukai Shi, Jiarong Ou, Rui Chen, Ke Lin, Jiahao Wang, Boyuan Jiang, Haotian Yang, Mingwu Zheng, Xin Tao, et al. Koala-36m: A large-scale video dataset improving consistency between fine-grained conditions and video content. *arXiv preprint arXiv:2410.08260*, 2024. 1
- [52] Ruichen Wang, Zekang Chen, Chen Chen, Jian Ma, Haonan Lu, and Xiaodong Lin. Compositional text-to-image synthesis with attention map control of diffusion models. *arXiv preprint arXiv:2305.13921*, 2023. 2
- [53] Thaddäus Wiedemer, Prasanna Mayilvahanan, Matthias Bethge, and Wieland Brendel. Compositional generalization from first principles. *Advances in Neural Information Processing Systems*, 36:6941–6960, 2023. 2, 3

- [54] Shuang Wu, Youtian Lin, Feihu Zhang, Yifei Zeng, Jingxi Xu, Philip Torr, Xun Cao, and Yao Yao. Direct3d: Scalable image-to-3d generation via 3d latent diffusion transformer. *arXiv preprint arXiv:2405.14832*, 2024. [1](#)
- [55] Divin Yan, Lu Qi, Vincent Tao Hu, Ming-Hsuan Yang, and Meng Tang. Training class-imbalanced diffusion model via overlap optimization. *arXiv preprint arXiv:2402.10821*, 2024. [2](#), [3](#)
- [56] Qihang Yu, Mark Weber, Xueqing Deng, Xiaohui Shen, Daniel Cremers, and Liang-Chieh Chen. An image is worth 32 tokens for reconstruction and generation. *Advances in Neural Information Processing Systems*, 37:128940–128966, 2024. [1](#)
- [57] Longwen Zhang, Ziyu Wang, Qixuan Zhang, Qiwei Qiu, Anqi Pang, Haoran Jiang, Wei Yang, Lan Xu, and Jingyi Yu. Clay: A controllable large-scale generative model for creating high-quality 3d assets. *ACM Transactions on Graphics (TOG)*, 43(4):1–20, 2024. [1](#)
- [58] Tianjiao Zhang, Huangjie Zheng, Jiangchao Yao, Xiangfeng Wang, Mingyuan Zhou, Ya Zhang, and Yanfeng Wang. Long-tailed diffusion models with oriented calibration. In *The twelfth international conference on learning representations*, 2024. [3](#)
- [59] Yifan Zhang, Bingyi Kang, Bryan Hooi, Shuicheng Yan, and Jia Shi Feng. Deep long-tailed learning: A survey. *IEEE transactions on pattern analysis and machine intelligence*, 45(9):10795–10816, 2023. [3](#), [6](#)
- [60] Juntu Zhao, Junyu Deng, Yixin Ye, Chongxuan Li, Zhijie Deng, and Dequan Wang. Lost in translation: Latent concept misalignment in text-to-image diffusion models. In *European Conference on Computer Vision*, pages 318–333. Springer, 2024. [2](#), [3](#), [7](#), [8](#)

# Imbalance in Balance: Online Concept Balancing in Generation Models

## Supplementary Material

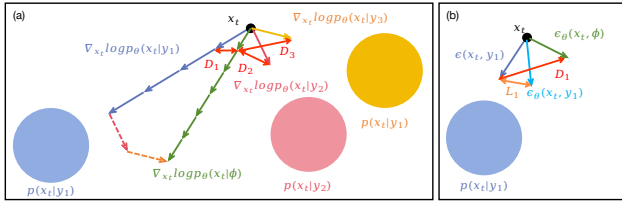


Figure 9. **Formulation of IMBA distance.** (a) **Unconditional** distribution shifts toward **head** concepts due to data imbalance, leading to a smaller IMBA distance  $D$  for head concepts. (b) Relationships between IMBA distance and diffusion loss during training.

### A. Formulation of IMBA Distance

Based on the above analysis, we can formulate the IMBA distance under the imbalanced data during training in Figure 9. As shown in Figure (a), starting from the random noise  $x_t$  in the latent space, conditional distribution points to different data distributions with different color based on different concepts. Due to data imbalance, concept  $y_1$  has far more samples than other concepts. Since the unconditional distribution is weighted by all samples equally during training, it will shift toward concepts with more samples like the green arrow, leading to a smaller IMBA distance  $D_1$ . In the training set, the ratio of samples between head and tail concepts often reaches a factor of thousands, far exceeding the ratio shown in the figure, indicating a much more severe data imbalance issue and more pronounced pattern of IMBA distance. As shown in Figure (b), original diffusion loss represents the distance between the conditional distribution and the predicted conditional distribution, and IMBA distance represents the distance between the predicted conditional distribution and the unconditional distribution. Specifically, when IMBA distance is implemented with the L2 norm, it is equivalent to the unconditional loss.

### B. Ablation study

#### B.1. Stability of IMBA Distance

In Figure 10, we calculate the IMBA distance of the same prompt on models with different size, architecture and noise. We find it is stable across all settings.

#### B.2. Comparison with Frequency-based Method

Since the text is a joint distribution of multiple concepts, it is difficult to calculate weights from a frequency perspective, and there is little concept-balancing work for text-to-image generation. Therefore, we compare IMBA loss with a frequency based method on class-image [9]. We sample 5 concepts each from the head and tail concepts and com-

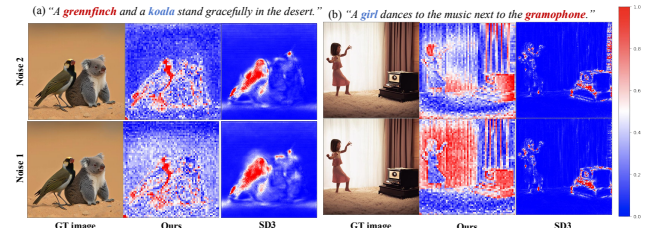


Figure 10. **IMBA distance of different models and noises.**

	Loss weight	Baseline	Frequency-based	Ours
Success rate	33.3%	49.3%	65.7%	
CLIP Score	0.3113	0.3101	0.3218	

Table 4. The performance of different balancing methods.

	Loss weight	Baseline	Sample-wise	Token-wise
Success rate	32%	64%	72%	
CLIP Score	0.2924	0.3022	0.3106	

Table 5. The performance of models with different loss weight.



Figure 11. The performance of models with different loss weight.

bine the data containing these concepts in the training set into a new subset. We then finetune the model on the subset using the frequency-based and our method respectively. Meanwhile, we pair the 10 concepts to generate 5 captions for each pair as the test set. As shown in the Table 4, our method outperforms the frequency-based method.

#### B.3. Comparison with Sample-wise Loss Weight

We finetune the same model on the imbalanced "piano-submarine" subset for 10K steps with sample-wise and our token-wise loss weight respectively. As shown in Table 5 and Figure 11, all results are evaluated on 25 captions. And sample-wise loss weight performs better than the baseline due to the reweight balancing. Meanwhile, token-wise loss weight achieves the best performance since it applies more fine-grained weights on different image regions according to concepts.

#### B.4. Hyper-parameters of IMBA Loss

We train the model on the "piano-submarine" subset to conduct ablation experiments on the value of  $\gamma$ . Specifically, when  $\gamma = 0.0$ , IMBA loss is equivalent to the original dif-

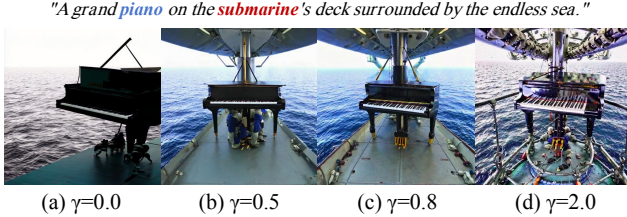


Figure 12. Results from models trained with different  $\gamma$ .

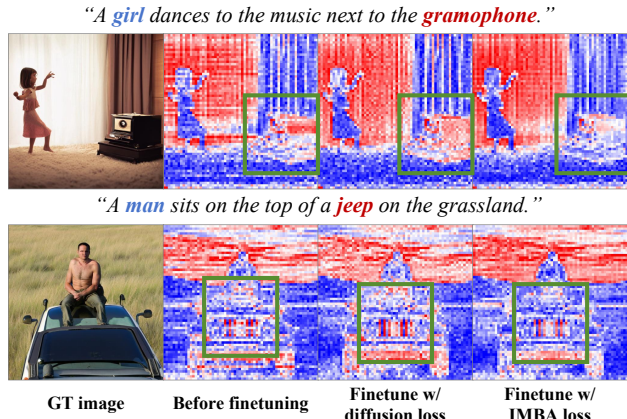


Figure 13. IMBA distance before and after finetuning.

fusion loss. When  $\gamma = 2.0$ , the value of the IMBA distance equals the value of the unconditional loss. As shown in Figure 12, when  $\gamma$  approaches 0.0, the concept composition ability of the model diminishes, as the semantic of the submarine in Figure(a) almost disappears. When  $\gamma$  approaches 2.0, the model exhibits severe color shift issues as seen in Figure(b). We chose  $\gamma = 0.8$  based on these observations.

### B.5. IMBA Distance after Training.

We resumed training a model for 3 epochs using diffusion loss, and then fine-tuned it separately with diffusion loss and IMBA loss. The difference in IMBA distance between the two models after fine-tuning is shown in Figure 13. It can be observed that, due to concept balancing during the training process with IMBA loss, the IMBA distance after training with IMBA loss pays more attention to tail concepts (red words). Consequently, the IMBA distance in the corresponding regions (green boxes) is smaller compared to training with diffusion loss.

## C. More Experiment Results of the Model Size

When testing different model sizes on the same dataset in Section 3, we observed that even with significant differences in model size, the generated images exhibit highly similar structural features given the same initial noise and text prompts, as illustrated in Figure 14. This suggests that once a model reaches a certain size, the dataset itself becomes more influential in determining the generated images rather than the model capacity. Larger models indeed have



Figure 14. Generation results of models with different sizes from the same initial noise.

better convergence capabilities, but they do not dictate the high-dimensional semantics or concept composition abilities of the images.